BULLETIN OF THE POLISH ACADEMY OF SCIENCES
TECHNICAL SCIENCES, Vol. 66, No. 3, 2018
DOI: 10.24425/123438

Mid-wave InAs/GaSb superlattice barrier infrared detectors with nBnN and pBnN design

E. GOMÓŁKA[1]*, O. MARKOWSKA[1], M. KOPYTKO[1], A. KOWALEWSKI[1], P. MARTYNIUK[1], A. ROGALSKI[1], J. RUTKOWSKI[1], M. MOTYKA[2], and S. KRISHNA[3]

[1] Institute of Applied Physics, Military University of Technology, 2 Kaliskiego St., 00-908 Warsaw, Poland
[2] Laboratory for Optical Spectroscopy of Nanostructures, Department of Experimental Physics, Wrocław University of Technology, 27 Wybrzeże Wyspiańskiego St., Wrocław, Poland
[3] Department of Electrical and Computer Engineering, Ohio State University, Columbus, Ohio 43210, USA

Abstract. We present an investigation of optical and electrical properties of mid-wavelength infrared (MWIR) detectors based on InAs/GaSb strained layer superlattices (SLs) with nBnN and pBnN design. The temperature-dependent behavior of the bandgap was investigated on the basis of absorption measurements. A 50% cut-off wavelength of around 4.5 μm at 80 K and increase of up to 5.6 μm at 290 K was found. Values of Varshni parameters, zero temperature bandgap E_0 and empirical coefficients α and β were extracted. Arrhenius plots of dark currents of nBnN and pBnN detectors were compared with the p-i-n design. Dark current density reduction in nBnN and pBnN detectors is observed in comparison to the p-i-n device. This shows a suppression of Shockley-Read-Hall (SRH) processes by means of introducing barrier architecture.

Key words: InAs/GaSb type-II superlattices, infrared detectors, barrier detectors, nBn detector, p-i-n detector.

1. Introduction

The InAs/GaSb type-II superlattice (T2SL) technology has recently experienced significant development in infrared (IR) technology. The operating wavelength of the T2SLs can be tailored from 3 μm to 32 μm, by varying thickness of one or two InAs/GaSb SL constituent layers [1–5], and can be considered an alternative to HgCdTe material both for the mid- (MWIR) and long-wavelength infrared (LWIR) range. Additionally, T2SL material systems can have some advantages over bulk HgCdTe, such as lower leakage currents and greater uniformity [6,7]. In contrast with HgCdTe, the effective masses are not directly dependent on bandgap energy. The electron effective mass of InAs/GaSb SLs is larger $m^*/m_o \approx 0.02$–0.03 as compared with $m^*/m_o = 0.009$ in HgCdTe alloy with the same bandgap $E_g \approx 0.1$ eV. Thus, tunneling currents in the T2SL detectors can be reduced in comparison with the HgCdTe alloy. What is more, large splitting between heavy-hole and light-hole valence subbands due to strain in the T2SLs contributes to suppression of Auger recombination. At the present stage of development, the residual doping concentration in an active region of InAs/GaSb SLs is around 1 to 2×10^{16} cm^{-3}, which indicates much higher doping than in HgCdTe materials (typically 10^{15} cm^{-3}). Higher doping at relatively short carrier lifetime points to a relatively low diffusion current. The measured carrier lifetime is typically below 100 ns and is limited by the Shockley-Read-Hall (SRH) mechanism. Therefore, the promise of Auger suppression has not yet been observed in practical device material. More recently, increase in the minority carrier lifetime to 157 ns has been observed due to incorporation of an InSb interfacial layer in InAs/GaSb SL [8]. The origin of the above recombination centers has been attributed to the presence of gallium, as the gallium-free InAs/InAsSb superlattices possess much longer lifetimes, up to 10 μs for undoped material in the MWIR region [9].

Short carrier lifetime, associated with the SRH mechanism, is the main limitation of the T2SL photodetectors based on the p-i-n (P-i-N) design. Device passivation is yet another problem caused by breaking the structure of periodic SLs on the lateral sides of the etched "mesa" structure [10–15]. Several materials and processes have been explored for device passivation, with some of the more prominent thin films studied including SiO_2, Si_3N_4 and AlGaSb. The best results have been achieved using polyimide passivation and inductively coupled plasma dry etching.

A class of IR detectors known as barrier detectors has shown promising results in eliminating the generation-recombination (GR) currents associated with SRH centers and mesa lateral surface imperfections, which have resulted in an increase of operating temperature [16] in comparison with the p-i-n design. A selection of their suggestions is shown in Fig. 1. These *X*Bn structures, so called after Klipstein *et. al* [17, 18], consist of an n- or p-type cap contact and an n-type absorber layer separated by a thin wide bandgap barrier (B). A unipolar barrier blocks one carrier type (electrons) but allows unimpeded flow of the other (holes). The introduction of a unipolar barrier into various configurations of photovoltaic structures suppresses dark current and noises without impending photocurrent flow. In particular, the barrier layer includes a passivation layer, suppressing the surface leakage current itself.

*e-mail: e.gomolka93@gmail.com

Manuscript submitted 2017-03-27, revised 2017-07-14, initially accepted for publication 2017-07-24, published in June 2018.

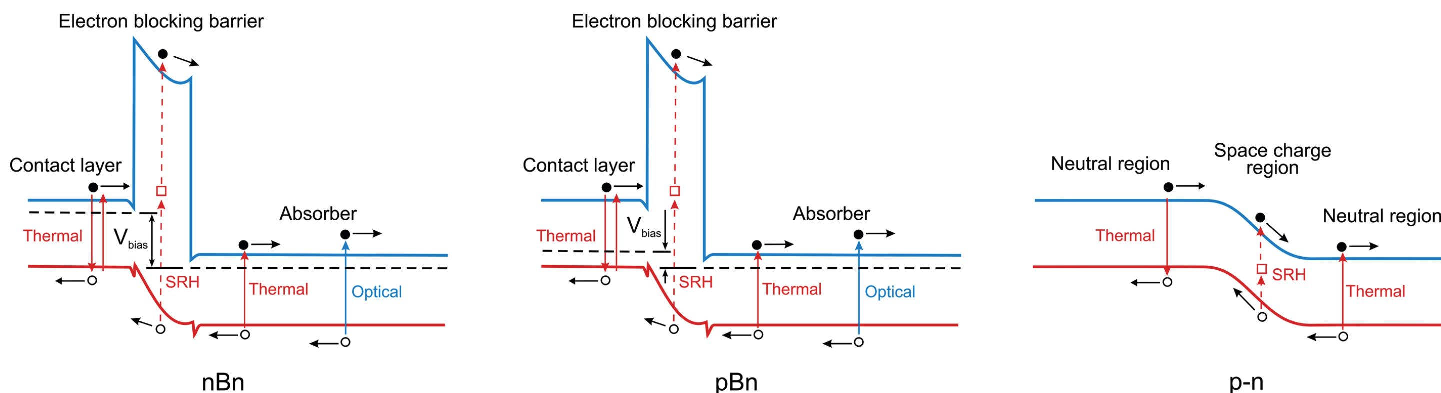

Fig. 1. Illustrations of bandgap diagram of nBn and pBn barrier detectors, and a p-n photodiode

However, the best solution is to use complementary barriers, i.e. to form a barrier for electrons and a barrier for holes at different depths. This structure was proposed by Ting *at al.* in 2009 and is known as the complementary barrier infrared device (CBIRD) [19]. These barriers allow a large part of the electric field to drop across the wider bandgap barrier materials, which in turn reduces the dark current associated with GR currents, tunneling currents, and the activity of SRH centers in the absorber region.

The idea of barrier detectors was proposed for the bulk material, however its introduction into SLs has allowed implementation of the barrier concept with greater control of arrangement of optimum band structure. Implementation of nBn design for the InAs/GaSb SL material system has been reported both for the MWIR [21–22] as well as LWIR [2, 3, 23, 24] range.

In the present work, investigation of optical and electrical properties of the MWIR *X*Bn InAs/GaSb SL detector design with the n- and p-type cap contact layer is presented. The properties of barrier detectors are compared with the p-i-n design.

2. Detectors design

Devices were grown on Te-doped epi-ready (100) GaSb substrates using a solid source molecular beam epitaxy (MBE) VG-80 system located at the Center for High Technology Materials, University of New Mexico laboratory. The system is equipped with SUMO effusion cells for gallium and indium, a standard effusion cell for aluminum and cracker cells for antimony and arsenic. Generally, analyzed barrier detectors consisted of four main layers. Details of the nBnN and pBnN detector structure are presented in Fig. 2. Following the growth direction, just behind the buffer layer, a 1.23 μm-thick N-type bottom contact layer was formed by 5 monolayer (ML) InAs/8 ML GaSb SLs doped with Si at the level of 2×10^{18} cm^{-3}. Then a 1.97 μm-thick non-intentionally doped (n.i.d.) absorber region formed by 8 ML InAs/8 ML GaSb SLs was grown, followed by a 210-nm-thick 9 ML AlSb/3 ML GaSb SLs barrier layer. The electron-blocking barrier layer was nominally undoped. Cap contact with a thickness of 400 nm is formed by

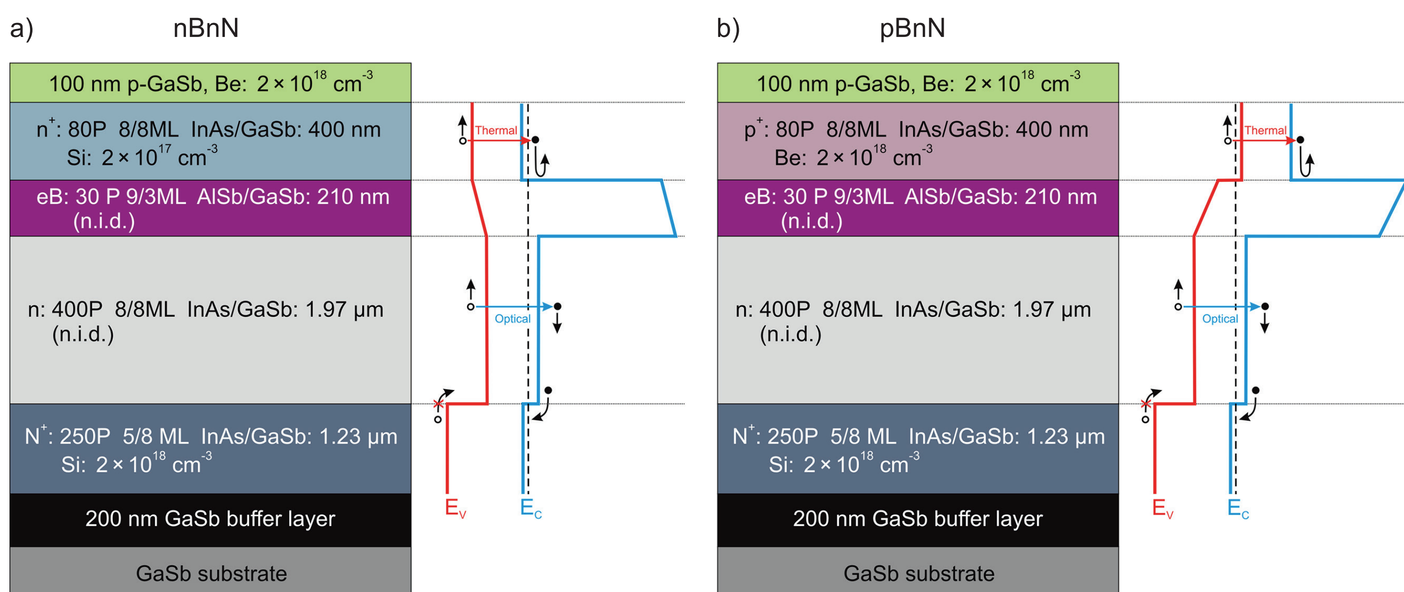

Fig. 2. Illustration of the layer-by-layer cross-section of detector structure and schematic band diagram of the nBnN (a) and pBnN (b) structures

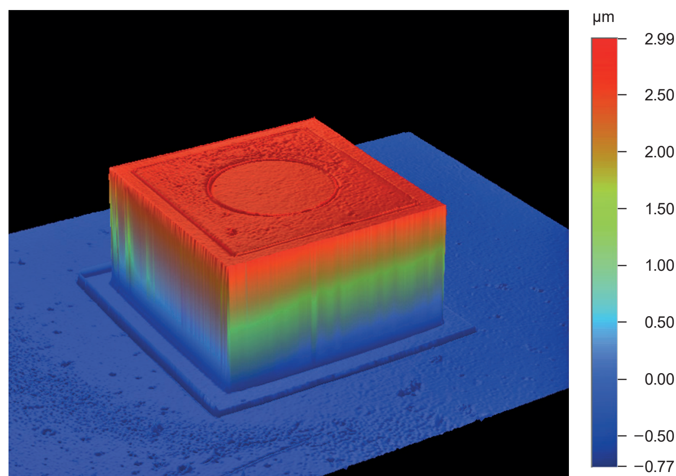

Fig. 3. 3D profile of a 400×400 μm square mesa-geometry T2SL detector after wet chemical etching and metallization

8 ML InAs/8 ML GaSb SLs doped with Si at the level of 2×10^{17} cm^{-3} in nBnN design and doped with Be at the level of 2×10^{18} cm^{-3} in pBnN design. The contact layer was capped with a 100-nm-thick p-GaSb to avoid oxidation during the processing steps and to improve ohmic contact properties.

8/8 ML InAs/GaSb SLs was chosen to adjust the active layer to the 4 ~ 5 μm wavelength range. Parameters of the adjacent layers were chosen by tailoring band offsets to achieve optimum performance. The wider bandgap electron barrier has been designed to provide a barrier from electron diffusion from the n-type (p-type) cap contact layer into the absorber region, yet allowing unimpeded flow of holes from the active region to the contact during reverse bias operation. Wider-bandgap bottom contact layer was chosen to create an exclusion junction preventing the injection of holes. To help visualize the expected band structure from this growth sequence, a conceptualization of it is also provided in Fig. 2, showing the device's expected mode of operation under illumination.

The devices were processed using 400×400 μm square mesas (Fig. 3). The shapes of detectors were defined by means of standard optical photolithography and wet chemical etching using $H_3PO_4 + C_6H_8O_7 + H_2O_2 + H_2O$ (1:1:4:16). Finally, Au was used as contact metal for both top and bottom contacts. Top contacts were formed with apertures ranging from 50 to 300 μm for front-side illuminating. Mesa slopes were not passivated. After fabrication, temperature-dependent spectral response and current density measurements as a function of bias voltage were conducted.

3. Results and discussion

Spectral response measurements for these devices were performed using a PerkinElmer Fourier transform infrared (FTIR) spectrometer in conjunction with a low-noise transimpedance preamplifier. The relative current responsivity versus wavelength plotted at a wide range of temperatures for the nBnN and pBnN SL detectors are shown in Fig. 4. The spectral response curves indicate a 50% cut-off wavelength of around 4.5 μm at 80 K and 5.6 μm at 290 K, which effectively covers the MWIR transmission window. The 50% cut-off wavelength of the response spectrum corresponds to

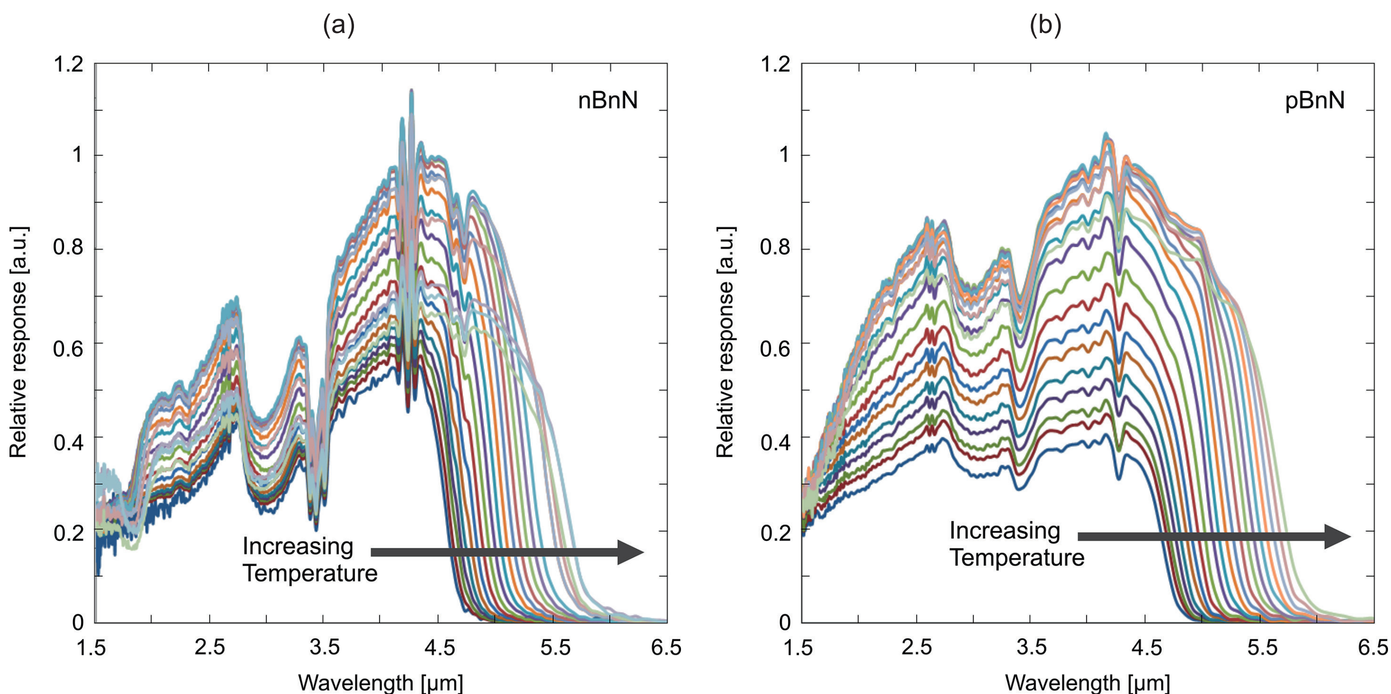

Fig. 4. Relative spectral response for temperatures 80–290 K of the MWIR nBnN (a) and pBnN (b) detectors measured at –0.1V. The cutoff wavelength increases with temperature

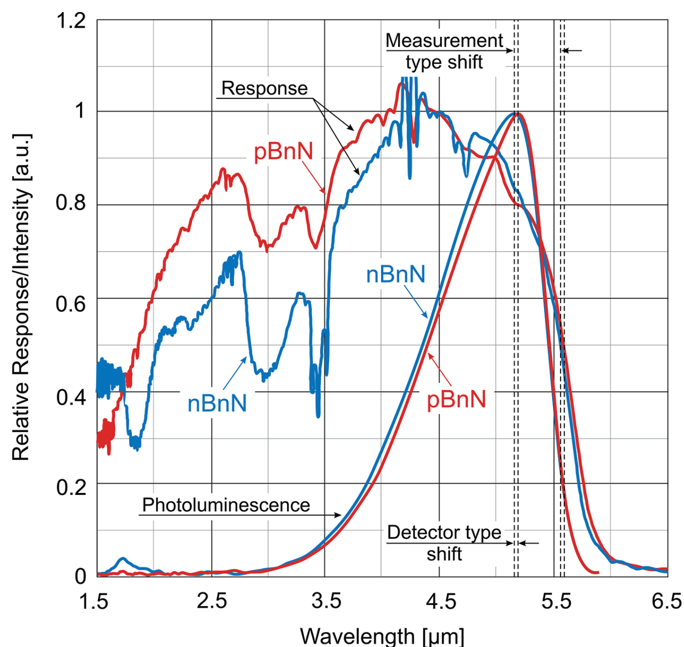

Fig. 5. Response and photoluminescence (PL) spectra at 293 K of the MWIR nBnN and pBnN detectors

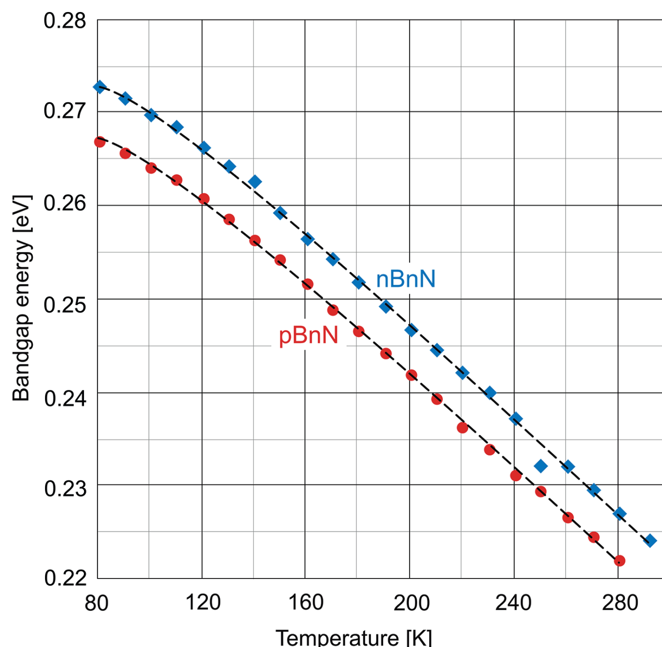

Fig. 6. Peak current responsivity versus reverse bias for the MWIR nBnN and pBnN detectors operating at 80 K. Devices were front-side illuminated through a 250 μm ring in metal contact

the maximum of the photoluminescence (PL) curve measured at room temperature (Fig. 5). However, the slight difference between values of the 50% cut-off wavelength and the maximum of the PL curve is visible. This is probably due to the band-filling effects caused by the different number of carriers created by different light sources in those two measurements, similarly as in Ref. [25]. Lasers in PL measurement, in contrast with the low power glow-bar sources in response measurement, excite many carriers from the hole subbands to the conduction subband, which fills the low-energy states within the band so that the bandgap appears widened. Moreover, a very small shift in wavelength, the same for both measurements, is visible for the nBnN and pBnN SL detectors. Active layers of both devices were formed by the same 8 MLs InAs/8 MLs GaSb SL, however we attribute this to variations in the quality of the samples.

Figure 6 shows peak current responsivity versus reverse bias of the detectors. Responsivity is shown to be enhanced by reverse biases. The nBnN device begins to be sensitive to IR radiation for voltages above –0.1 V, while for the pBnN device this voltages stands at above –0.2 V. The increased bias needed to operate this devices lends evidence to the presence of an unintended valence band barrier that must be overcome with an appreciable bias before efficient flow of photo-excited carriers is possible. What is more, the values of current responsivity are not so high. For the front-side, the devices were illuminated through a 250 μm ring in metal contact. For this geometry, the current responsivity is calculated based on the optical area instead of the junction area, assuming that photo-generated carriers are only contributed by the direct illuminated regions. Both devices, with their wider-gap bottom contact layer, are also designed to be backside illuminated. Backside illumination may yield higher current responsivities. However, the requirement is to use transparent substrates for IR radiation, for example GaAs. Recently, Martyniuk *et al.* [26] have presented the performance of the MWIR InAs/GaSb SL with a bulk AlGaSb barrier nBn detector on a GaAs substrate. To accommodate the 7.8% lattice mismatch between detector structure and the GaAs substrate, the interfacial misfit dislocation (IMF) array and GaSb buffer layers were introduced. The 1.1-mm-thick GaAs substrate was converted into an immersion lens to limit the influence of the defects occurring during growth on GaAs substrate, and to increase detectivity.

The bandgap of active layer was determined on the basis of response measurements and the cut-off was defined at the wavelength where the signal was reduced to 50% of its peak value. The bandgap of 8 MLs InAs/8 MLs GaSb SL was found to be of about 0.27 eV at 80 K and decreasing with temperature. Temperature dependence of the $A_{III}B_V$ binary compounds bandgap E(T) can be approximated by the Varshni relation [27]:

$$E(T) = E_0 - \alpha T^2/(T+\beta), \qquad (1)$$

where E_0 is the bandgap at 0 K, and α and β are fitting parameters characteristic of a given material. Table 1 shows the best fit values of parameters E_0, α and β for nBnN and pBnN detectors. The exemplary fits obtained are shown in Fig. 7. The zero temperature bandgap of 0.306 eV of the pBnN detector is slightly lower than the one of the nBnN detector, which equals 0.311 eV. This is due to a shift in wavelength (see Fig. 5) caused by variations in the quality of samples. The change of bandgap

Table 1
Extracted Varshni parameters for the MWIR nBnN and pBnN SL detectors

Detector	E0 [eV]	α [meVK^{-1}]	β [K]
nBnN	0.311	0.262	–36.083
pBnN	0.306	0.261	–37.321

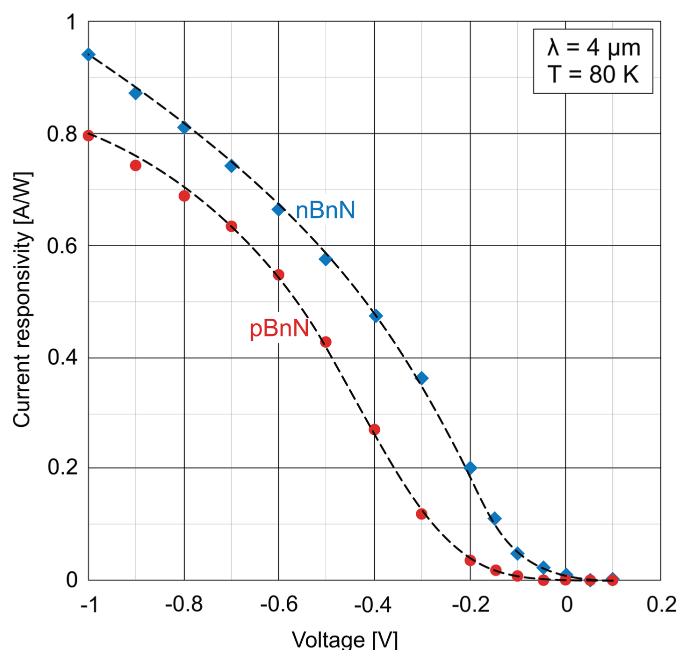

Fig. 7. Energy bandgap versus temperature of the MWIR nBnN and pBnN detectors

with temperature for both types of detectors is the same. It was found that the bandgap in the 8 MLs InAs/8 MLs GaSb SL changed on average by 0.26 meVK^{-1}. This α parameter is about two times lower than for InAs (0.6 meVK^{-1}) [28]. Thus β, which is supposed to be related to the Debye temperature, may in certain important cases be negative [27].

Figure 8 shows the plots' current-voltage characteristics versus temperature 80–290 K of the MWIR nBnN and pBnN detectors. The current–voltage characteristics have been measured using the Agilent B2902A sourcemeter. Negative bias corresponds to reverse bias, i.e. when negative voltage is applied to the n$^+$ or p$^+$ cap contact, the unipolar barrier blocks the flow of the electron current from the n$^+$ or p$^+$ region, which should allow the collection of thermally and optically generated holes from the absorber. However, the "turn-on" voltage of about –0.75 V at 80 K for the nBnN detector. specific for barrier devices, is visible, confirming the presence of an unintended valence band barrier (see also Fig. 6). The "turn-on" voltage moves towards lower reverse biases with increasing temperature. At higher temperatures, dark currents of both nBnN and pBnN detectors are comparable. At low temperatures, the pBnN detector shows slightly lower dark current densities. At this temperatures, measurements are limited by the noise floor of the measurement setup.

Arrhenius plots of the analyzed T2SL detectors, of current density of – 1 V, are depicted in Fig. 9. nBnN and pBnN detectors are compared with the p-i-n design. The p-i-n detector was also grown using the MBE method on the GaSb substrate. Absorber region formed by 8 MLs InAs/8 MLs GaSb SL is the same as in the analyzed barrier devices. The dashed line shows the level of matching the form of the temperature dependence dark current:

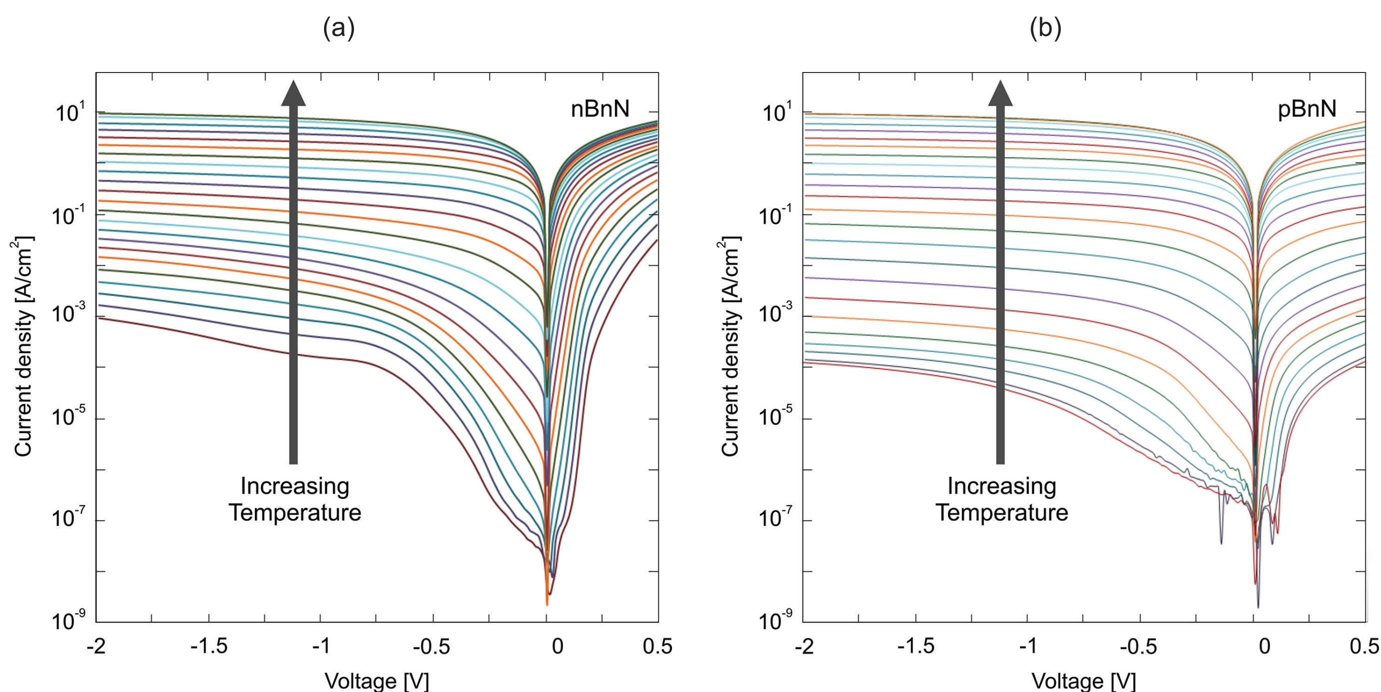

Fig. 8. Current-voltage characteristics versus temperature of 80–290 K of the MWIR nBnN (a) and pBnN (b) detectors

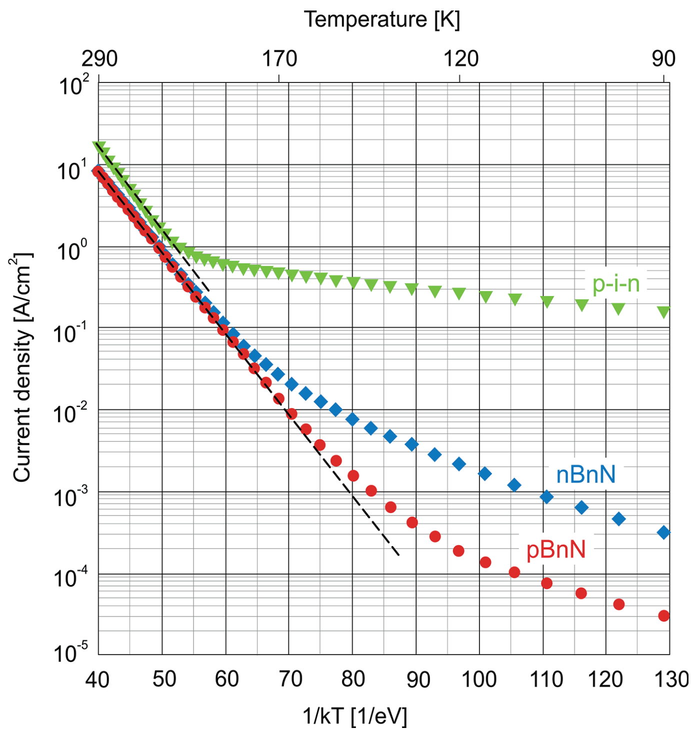

Fig. 9. Arrhenius plot of the dark current of the MWIR nBnN and pBnN SL detectors as compared with the p-i-n SL design. Data was plotted at –1 V

$$J_{DARK}(T) \propto \exp\left(\frac{-E_a}{k_B T}\right), \tag{2}$$

where E_a is the activation energy and k_B is the Boltzmann constant. An exponential fit to the data gives activation energy of about 0.225 eV, which is close to the bandgap of the 8 MLs InAs/8 MLs GaSb SL at room temperature. This shows a suppression of SRH processes above approximately 210 K in the p-i-n device. Although detectors with the *X*Bn design were fabricated at standard mesa geometry, suppression in the dark current density at 170 K greater than one order of magnitude is observed. However, at lower temperatures, activation energy for detectors with the *X*Bn design is close to 50 meV. This reveals the dominant mechanism behind surface leakage or tunneling currents.

4. Conclusions

The temperature-dependent behavior of the MWIR detectors based on InAs/GaSb SL with nBnN and pBnN design have been investigated. Values of Varshni parameters for 8 MLs InAs/8 MLs GaSb SL absorbing layers were extracted. Zero temperature bandgap of 0.306 eV was found for the pBnN detector and of 0.311 eV for the nBnN detector. We attribute this slight difference to variations in the quality of the samples. The bandgap changed on average by 0.26 meVK^{-1}.

Arrhenius plots of the current density of the nBnN and pBnN SL detectors were compared with the p-i-n design. Activation energy of about 0.225 eV at –1 V was found. This value is close to the bandgap of the 8 MLs InAs/8 MLs GaSb SL at room temperature. In the p-i-n device, a suppression of SRH processes is visible above approximately 210 K. Below this temperature, nBnN and pBnN detectors exhibit much lower values of dark current density. A deviation from diffusion to GR-limited behavior of barrier devices is visible for temperatures below 170 K.

Significant dependence of current responsivity on reverse bias, as well as large "turn-on" voltages both evidence the presence of an unintended valence band barrier that must be overcome with relatively high bias before efficient flow of photo-excited carriers becomes possible. In order to compensate for this valence band barrier, more rigorous bandgap engineering and control of doping levels are needed.

Acknowledgements. We wish to thank the National Science Centre of Poland for their support in the form of grant No. UMO-2015/19/B/ST7/02200 and the National Centre for Research and Development (Poland), for their grant No. POIR.04.01.04–00–0027/16.

References

[1] C. Cervera, I. Ribet-Mohamed, R. Taalat, J. P. Perez, P. Christol, and J. B. Rodriguez, "Dark current and noise measurements of an InAs/GaSb superlattice photodiode operating in the midwave infrared domain", *J. Electron. Mater.* 41, 2714–2718 (2012).

[2] N. Gautam, H.S. Kim, M.N. Kutty, E. Plis, L. R. Dawson, and S. Krishna, "Performance improvement of longwave infrared photodetector based on type-II InAs/GaSb superlattices using unipolar current blocking layers", *Appl. Phys. Lett.* 96, 231107 (2010).

[3] Y. Wei, A. Gin, M. Razeghi, and G.J. Brown, "Advanced InAs/GaSb superlattice photovoltaic detectors for very long wavelength infrared applications", *Appl. Phys. Lett.* 80, 3262–3264 (2002).

[4] E. Plis, "InAs/GaSb Type-II Superlattice Detectors", *Advances in Electronics* 246769 (2014).

[5] A. Rogalski, M. Kopytko, and P. Martyniuk, "InAs.GaSb type-II superlattice infrared detectors: three decades of development", *Proc. of SPIE* 10177, 1017715 (2017).

[6] D.L. Smith and C. Mailhiot, "Proposal for strained type II superlattice infrared detectors", *J. Appl. Phys.* 62, 2545–48 (1987).

[7] C. Mailhiot, "Far-infrared materials based on InAs/GaInSb type II, strained-layer superlattices", in *Semiconductor Quantum Wells and Superlattices for Long-Wavelength Infrared Detectors,* ed. M. O. Manasreh, 109–38, Artech House, Boston, MA, 1993.

[8] D. Zuo, P. Qiao, D. Wasserman, and S.L. Chuang, "Direct observation of minority carrier lifetime improvement in InAs/GaSb type-II superlattice photodiodes via interfacial layer control", *Appl. Phys. Lett.* 102, 141107 (2013).

[9] Y. Aytac, B.V. Olson, J.K. Kim, E.A. Shaner, S.D. Hawkins, J.F. Klem, M.E. Flatte, and T.F. Boggess, "Effects of layer thickness and alloy composition on carrier lifetimes in mid-wave infrared InAs/InAsSb superlattices", *Appl. Phys. Lett.* 105, 022107 (2014).

[10] E. Plis, M.N. Kutty, and S. Krishna, "Passivation techniques for InAs/GaSb strained layer superlattice detectors", *Laser Photonics Rev.* 7(1), 45–59 (2013).

[11] E.K. Huang, D. Hoffman, B.-M. Nguyen, P.-Y. Delaunay, and M. Razeghi, "Surface leakage reduction in narrow band gap type-II antimonide-based superlattice photodiodes", *Appl. Phys. Lett.* 94, 053506–1-3 (2009).

[12] R. Rehm, M. Walther, F. Fuchs, J. Schmitz, and J. Fleissner, "Passivation of InAs/(GaIn)Sb short-period superlattice photodiodes with 10 μm cutoff wavelength by epitaxial overgrowth with $Al_xGa_{1-x}As_ySb_{1-y}$", *Appl. Phys. Lett.* 86, 173501–1–3 (2005).

[13] P.Y. Delaunay, A. Hood, B.M. Nguyen, D. Hoffman, Y. Wei, and M. Razeghi, "Passivation of type-II InAs/GaSb double heterostructure", *Appl. Phys. Lett*. 91, 091112–1-3 (2007).

[14] G. Chen, B.-M. Nguyen, A.M. Hoang, E.K. Huang, S.R. Darvish, and M. Razeghi, "Elimination of surface leakage in gate controlled type-II InAs/GaSb mid-infrared photodetectors", *Appl. Phys. Lett*. 99, 183503 (2011).

[15] R. Rehm, F. Lemke, M. Masur, J. Schmitz, T. Stadelmann, M. Wauro, A. Wörl, and M. Walther, "InAs/GaSb superlattice infrared detectors", *Infrared Phys. Technol.* 70, 87–92 (2015).

[16] S. Maimon and G. Wicks, "nBn detector, an infrared detector with reduced dark current and higher operating temperature", *Appl. Phys. Lett.* 89, 151109–1–3 (2006).

[17] P. Klipstein, "*X*B*n*" barrier photodetectors for high sensitivity and high operating temperature infrared sensors", *Proc. of SPIE* 6940, 69402U (2008).

[18] P. Klipstein, O. Klin, S. Grossman, N. Snapi, B. Yaakobovitz, M. Brumer, I. Lukomsky, D. Aronov, M. Yassen, B. Yofis, A. Glozman, T. Fishman, E. Berkowicz, O. Magen, I. Shtrichman, and E. Weiss, "XBn barrier detectors for high operating temperatures", *Proc. of SPIE* 7608, 76081V (2010).

[19] D.Z. Ting, A. Soibel, J. Nguyen, C.J. Hill, S.A. Keo, J.M. Mumolo, and S.D. Gunapala, "A high-performance long wavelength superlattice complementary barrier infrared detector", *Appl. Phys. Lett.* 95, 023508 (2009).

[20] A. Khoshakhlagh, J.B. Rodriguez, E. Plis, G.D. Bishop, Y.D. Sharma, H.S. Kim, L.R. Dawson, and S. Krishna, "Bias dependent dual band response from InAs/Ga(In)Sb type II strain layer superlattice detectors", *Appl. Phys. Lett.* 91, 263504 (2007).

[21] J.B. Rodriguez, E. Plis, G. Bishop, Y.D. Sharma, H. Kim, L.R. Dawson, and S. Krishna, "nBn structure based on InAs/GaSb type-II strained layer superlattices", *Appl. Phys. Lett.* 91, 043514 (2007).

[22] H.S. Kim, E. Plis, J.B. Rodriguez, G.D. Bishop, Y.D. Sharma, L.R. Dawson, S. Krishna, J. Bundas, R. Cook, D. Burrows, R. Dennis, K. Patnaude, A. Reisinger, and M. Sundaram, "Mid-IR focal plane array based on type-II InAs/GaSb strain layer superlattice detector with nBn design", *Appl. Phys. Lett.* 92, 183502 (2008).

[23] A. Khoshakhlagh, S. Myers, H.S. Kim, E. Plis, N. Gautam, S.J. Lee, S.K. Noh, L.R. Dawson, and S. Krishna, "Long-wave InAs/GaSb superlattice detectors based on nBn and Pin designs", *IEEE J. Quant. Electron.* 46(6), 959–964 (2010).

[24] P.C. Klipstein, E. Avnon, D. Azulai, Y. Benny, R. Fraenkel, A. Glozman, E. Hojman, O. Klin, L. Krasovitsky, L. Langof, I. Lukomsky, M. Nitzani, I, Shtrichman, N. Rappaport, N. Snapi, E. Weiss, and A. Tuito, "Type II superlattice technology for LWIR detectors", *Proc. SPIE* 9819, 98190T (2016).

[25] B. Klein, E. Plis, M.N. Kutty, N. Gautam, A. Albrecht, S. Myers and S. Krishna, "Varshni parameters for InAs/GaSb strained layer superlattice infrared photodetectors", *J. Phys. D: Appl. Phys.* 44, 075102 (2011).

[26] P. Martyniuk, W. Gawron, D. Stępień, D. Benyahia, A. Kowalewski, K. Michalczewski, and A. Rogalski, "Demonstration of mid-wavelength type-II superlattice InAs/GaSb single pixel barrier detectors with GaAs immersion lens", *IEEE Electron Dev. Lett.* 37(1), 64-65 (2016).

[27] Y.P. Varshni, "Temperature dependence of the energy gap in semiconductors", *Physica* 34(1), 149–154 (1967).

[28] M. Levinstein, S. Rumyantsev, and M. Shur, *Handbook Series on Semiconductor Parameters* vol. 1 and 2 (London: World Scientific, 1999).